Velocity Control of Nonlinear Unmanned Rotorcraft using Polytopic Modelling and State Feedback Control

Reza Tarighi[1], Amir Hooshang Mazinan[2, *]
Department of Control Engineering, Faculty of Electrical Engineering, South Tehran Branch, Islamic Azad University, Tehran, Iran.
E-mail: st_r_tarighi@azad.ac.ir, mazinan@azad.ac.ir
*Corresponding author

Mohammad Hosein Kazemi[3]
Faculty of Electrical Engineering, Shahed University, Tehran, Iran.
E-mail: kazemi@shahed.ac.ir

Received: 27 October 2019, Revised: 18 January 2020, Accepted: 20 January 2020

Abstract: Performance and improvement of flight efficiency at various velocities for flight systems, in particular, rotorcrafts, with specific complexities in motion and its nonlinear equations are always of particular interest to researchers in the aerial and control domains. In this research, a new control algorithm is addressed based on the complete nonlinear Unmanned Rotorcraft (UR) model and its four main inputs. Exploiting state feedback and Polytopic Linear Parameter Varying (PLPV) modeling and using Linear Matrix Inequality (LMI), the velocity control problem is investigated. The trim points of the system are produced under different velocity control conditions. State feedback control gain matrix which plays a main role in producing the ultimate control signal, is computed by solving a set of LMIs under various conditions. Finally, instead of using a Nonlinear model, a Polytopic model is used for controller synthesis. With this goal, different scenarios for the proposed flight velocity control (in different dynamic ranges, minimum velocity to maximum velocity) are implemented. The simulation results demonstrate a very good performance of the proposed controller in the basis of PLPV modelling. It can be concluded that the proposed manner is useful to overcome the disruptions imposed on the flight system due to the changes in the equilibrium points and the uncertainties of the parameters and/or possible errors due to the unwanted possibilities in the system.

Keywords: Nonlinear Unmanned Rotorcraft, LMI, LPV, Polytopic Modelling

Reference: Reza Tarighi, Amir Hooshang Mazinan, and Mohammad Hosein Kazemi, "Velocity Control of Nonlinear Unmanned Rotorcraft using Polytopic Modelling and State Feedback Control", Int J of Advanced Design and Manufacturing Technology, Vol. 13/No. 3, 2020, pp. 33–49. DOI: 10.30495/admt.2020.1881971.1151.

Biographical notes: Reza Tarighi received his MSc in control engineering from the South Tehran Branch, Islamic Azad University, Tehran, Iran, in 2010. He is now a PhD student at South Tehran Branch, Islamic Azad University, Tehran, Iran. His current research interests include control analysis image processing, robotics, and aerospace. **Amir Hooshang Mazinan** received his PhD in 2009 in Control Engineering. He is an Associate Professor and also the Director of Control Engineering Department at Islamic Azad University, South Tehran Branch, Tehran, Iran, since 2009. He is now acting as the Associate Editor in Transactions of the Institute of Measurement and Control (Sage publisher) and Computers & Electrical Engineering Journal (Elsevier Publisher), as well. **Mohamad Hosein Kazemi** received his MSc and PhD in control engineering from the Sharif University of Technology, Tehran, Iran, and Amirkabir University, Tehran, Iran, in 1995 and 2001, respectively. He is currently an Associate Professor in the Department of Electrical Engineering at the Shahed University, Tehran, Iran.

1 INTRODUCTION

It has been years since the first attempts to fly and to build flight systems. During these years, attempts to construct various types of vehicles have developed with different flying features. These efforts led to the made of a flying device with special advantages in flying the helicopter or rotorcrafts name. In addition to the flight features of the aircraft, the characteristics include the ability to the rearward flight, hovering flight and sideward flight and vertical flight. The different usage of rotorcrafts relies on these capabilities, relief, and medical services, social and welfare services, aerial imaging, geology, and so on. The rotorcrafts are one of the most nonlinear and complex systems that are inherently unstable due to the flight performance system. This is mainly due to the fact that the rotor and fuselage are interconnected. the performance of operational rotorcrafts (actual) and unmanned rotorcrafts are approximately analogous in structure. However, because of the inexistence of accurate information on such helicopters(actual), the article focuses on unmanned rotorcrafts. Achieving the desired velocities by considering all four inputs simultaneously as well as involvement of the tail and the main rotor will improve the stability performance of the flight system even in the state of the momentary shock to the user or the flight system controller, (for the reasons mentioned above, nonlinear and complex systems and significant high impact of the main rotor and the tail rotor on each other and difficult conditions to consider at the same time all four of the main entrance to the helicopter).

This paper attempts to introduce different scenarios to examine different modes of speed. That is, we analyze them using unique capabilities LPVs, as well as solvers of Linear Matrix Inequalities (LMI). Effective and good research has been done on unmanned helicopters. But there has been less focus on velocity and movement maneuvers based on the authors' knowledge so far. Furthermore, if the research has been done, it has been more focused on the state (Hover or its surroundings). The research about the application LPVs, of the helicopter and UAV can be seen in[10-16]. This section introduces a summary of the study on research topics conducted in different scopes of rotorcrafts, especially unmanned rotorcrafts. In [1], controlling the nonlinear autonomous rotorcraft model is investigated that offers how to create a nonlinear model and a nonlinear control strategy for a rotorcraft. The proposed nonlinear model has some very specific characteristics that make it an interesting challenge in the investigation, even in the case of three degrees of freedom precisely, aerodynamic forces lead to signals and matrices that are notably considered in the contents of mechanical control systems. In [2], H_∞ control design has been investigated which is structured for steering and loop control of the unmanned rotorcraft that has a controller based design for the robust output feedback and, the reason for this choice is the simplicity of the proposed method in which the control gains are obtained from solving just two matrix coupling (pair) equations. Then, an efficient algorithm is presented for solving these two matrix equations in which we do not need sustained gain as an initial condition.

In [3], H_∞ robust control has been analyzed for an unmanned rotorcraft in the presence of uncertainties as well as applying wind disturbance as uncertainty in this flight model in static flight mode. In reference [4] as a review, an adaptive robust control design is investigated for unmanned rotorcraft in aerial vehicles based on a sliding mode approach in which the purpose of the study is to enable a rotorcraft to detect a position and the position different from the predetermined time. The suggested controller employes the feedback linearization process to control synthesis, it controls the adaptive sliding mode to compensate for the parametric uncertainty and external impairments. In [5], flying in a stable state is presented for an unmanned rotorcraft using fuzzy control for sustained flight in a small unmanned rotorcraft in turbulent air environments. The design of the controller includes two loops, an inner ring controller is presented for the angle and height, and an outer ring controller is produced, which is presented for the position control of the rotorcraft. In reference [6], tracking control problem is studied by using the adaptive robust control for an autonomous rotorcraft. In this study, a small unmanned rotorcraft system is exposed to input saturation and output constraints. The radial base function of the neural networks is used to satisfy the uncertainty of the system.

The rotorcraft system is provided to show the effectiveness of the tracking development plan using the disturbance. Reference [7] investigates nonlinear robust control which is based on disorder observations for a small-scale unmanned rotorcraft. The control goal is to let the rotorcraft follow a predetermined path. Proposing nonlinear robust control is based on the sliding mode control technique with the backstepping mode. The control function is different based on a time disturbance observer. The nonlinear model of the rotorcraft has been modified as a nonlinear dependent system to obtain a control rule. The mathematical proof using the Lyapunov function and the stability theorems show that the closed-loop system is completely stable in the presence of this controller. In [8], dynamic control optimization was sought for unmanned small scale rotorcraft, compared to several repetitious various search algorithms. Optimized parameters of chosen parameters are an artificial native cloning algorithm and an LQG controller is designed for a fair comparison of controller performance.

In [9] reference, the dynamic nonlinear inverse control design of an unmanned rotorcraft has been studied. The dynamic inverse design offers an ideal solution for flying rotorcraft control, which effectively separates the model and in particular controls the nonlinear model. However, regarding rotorcraft restrictions, this method requires complete state feedback. The control design study is done using dynamic reversal with reduced models.

Reviewing LPV control, we can point to the reference [10], which refers to the linear matrix inequalities based on nonlinear adaptive robust control for a small autonomous quadcopter. In this study, the design of the controller is used for various applications of a quadcopter, including precise tracking, independent routing navigation in the presence of disturbances, and delivery of the package without loss of performance. The design is based on the determination of the inner and the outer ring. In the study [11], a method for controlling the LPV model for reducing harmonic vibration on the top of the rotorcraft has been studied. In this research, the controller has been designed to reduce the stable vibration reduction throughout the rotorcraft effective flight path despite variations in vibrational and dynamic flight conditions. In [12], a comparative study is peresented and robustness analysis of quadrotor control in the presence of wind disturbances is investigated. In the study [13], the setting of the gain of the screw state of the linear variable parameter for a rotorcraft is presented which, in this reference, it has been investigated first as a schematic design of the screw state setting and finally, as the control of a linear class of (LPV).

Reference [14] can be referred to as an article entitled the robust linear variable parameter control algorithm by adjusting the gain for the laboratory quad-copter using a linear matrix which is based on the inequality (LMI) method. In this Reference, the design is proposed by a robust control technique of the LPV with an induced L2 norm efficiency. Different techniques of LPV control have been reported in this paper for design control with adjusting the gain on a nonlinear device, such as mode feedback with the limits of the polarization area, LPV control, the mode feedback, and LPV control. One disadvantage is that steady control over non-resistance parameters and disturbances are not as strong as most airborne and non-resistance industries with external disturbances.

Therefore, they are not suitable for every model. In [15], LQR control uses the LMI technique for an unmanned rotorcraft with the selection of the band domain that is based on the convexity. In [16], robust control is used for an unmanned rotorcraft with several inputs and outputs on the automatic flight and it is only studied in the investigation of a trend in the direction of the longitudinal direction, however, in this design, the examined aim of speed control is considered automatically. This process, at first, includes the introduction of rotorcraft modeling based on its dynamic and kinematic structure and then, based on the model, it is extracted according to the different rotorcraft speeds. In the next step, we introduce the polytypic LPV model which is based on the extraction of the flight system. In the next level, the LPV model is performed, based on the extracted model of the nonlinear and design controller that is based on solving the LMI equations and then, in the simulation section, introducing different scenarios in different speeds have been investigated for their stability and finally, conclusion and references are presented. Figure 1 presents the coordinates of the fuselage and the hub of a rotorcraft.

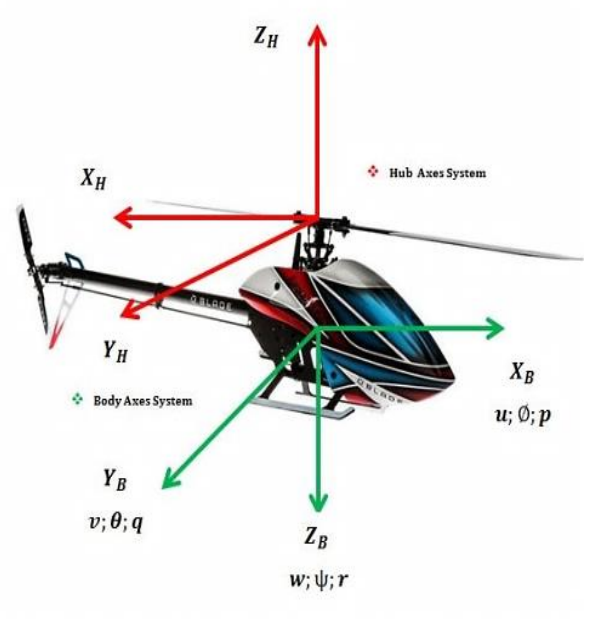

Fig. 1 Introducing the fuselage and the hub.

2 NONLINEAR DYNAMIC MODEL

All manuscripts are to be submitted online According to Newton's second law, the product of multiplication of mass in the acceleration is equal to force; it means that:

$$F = M\ a \tag{1}$$

According to Newton's second law, we will have [17]:

$$\vec{f} = m\frac{\overrightarrow{dv}}{\overrightarrow{dt}}:I \tag{2}$$

$$\frac{\overrightarrow{dv}}{\overrightarrow{dt}}:I = \frac{\overrightarrow{dv}}{\overrightarrow{dt}}:B + \vec{\omega}\times\vec{v} \tag{3}$$

The difference between "Eq. (2) and (3)" is that when they are implemented on a free space vector in space, the obtained result is generally different. If we recall equations in (1), by considering the rules governing the second rule and introducing $F_B : [F_x \ F_y \ F_z]^T$ and $M_B : [L \ M \ N]^T$, by using the mentioned kinematic equations, we will have "Eq. (4) and (5)" which consist of all external forces inserted, respectively, except for the gravity and moment forces around the axis of the roll and the screw or around the axes X, Y, Z. Using the kinematic equations that were mentioned before, we express "Eq. (4) and (5)".

$$m\dot{v}+m(\omega\times v)=F \tag{4}$$

$$I\dot{\omega}+(\omega\times I\omega)=M \tag{5}$$

By introducing $V_B=(u,v,\omega)^T$; $\omega^B_{B/N}=(p,q,r)^T$, they are angular and linear velocities relative to the structure of coordinate axes, respectively. In other words, it can be written as:

$$\begin{pmatrix}\dot{u}\\ \dot{v}\\ \dot{w}\end{pmatrix}=-\begin{pmatrix}p\\ q\\ r\end{pmatrix}\times\begin{pmatrix}u\\ v\\ w\end{pmatrix}+\left\{\begin{pmatrix}-g\sin\theta\\ g\sin\varnothing\cos\theta\\ g\cos\varnothing\cos\theta\end{pmatrix}+m^{-1}\begin{pmatrix}F_x\\ F_y\\ F_z\end{pmatrix}\right\} \tag{6}$$

Where their descriptive unit m/s stands for V_B and rad/s stands for $\omega^B_{(B/N)}$ and the symbole × is a cross-product [18]. If we define F_B in the form of "Eq. (7)" [19]:

$$\begin{aligned}F_x &= X_{mr}+X_{fus}\\ F_y &= Y_{mr}+Y_{fus}+Y_{tr}+Y_{vf}\\ F_z &= Z_{mr}+Z_{fus}+Z_{hf}\end{aligned} \tag{7}$$

$$\dot{V}_B=-\omega^B_{B/N}\times V_B+m^{-1}F_B+F_{BG} \tag{8}$$

If we express the moment equations in the form of the "Eq. (9)" with the explanation that L, M, N are the Moment of the roll and screw, or on the coordinate axes of the fuselage:

$$\begin{aligned}\dot{p}&=\frac{1}{I_{yy}I_{xx}-I_{xz}^2}\left\{qr\left(I_{yy}I_{zz}-I_{zz}^2-I_{xz}^2\right)+qpI_{xz}\left(I_{zz}+I_{xx}-I_{yy}\right)+LI_{zz}+NI_{xz}\right\}\\ \dot{r}&=\frac{1}{I_{yy}I_{xx}-I_{xz}^2}\left\{qrI_{xz}\left(I_{yy}-I_{zz}-I_{xx}\right)+qp\left(I_{xz}^2+I_{xx}^2-I_{xx}I_{yy}\right)+LI_{xz}+NI_{xx}\right\}\\ \dot{q}&=\frac{1}{I_{yy}}\left[pr\left(I_{zz}-I_{xx}^2\right)+I_{xz}\left(r^2-p^2\right)+M\right]\end{aligned} \tag{9}$$

According to this, moment relations can be presented in the form of:

$$\begin{aligned}L&=L_{mr}+L_{vf}+L_{tr}\\ M&=M_{hf}+M_{mr}\\ N&=N_{mr}+N_{vf}+N_{tr}\end{aligned} \tag{10}$$

Which for this equation, the symbols L_{mr}, N_{mr}, M_{mr} are defined as the moment around the screw to the moment produced in the main rotor, M_{hf} is defined as the aerodynamic moment produced by the horizontal wing, L_{vf}, N_{vf}, as the aerodynamic moment produced by the vertical wings and L_{tr}, N_{tr} as the aerodynamic moment produced by the tail rotor, respectively. The indecies $(\cdot)_{mr}, (\cdot)_{tr}, (\cdot)_{fus}, (\cdot)_{vf}, (\cdot)_{hf}$ represent the symbol of the main rotor and tail and fuselage rotor and the vertical and horizontal fins, respectively [19]. The values of the variables used in the paper are presented in "Table 1" [19] from the center of gravity (CG). In summary, the equation (9) can be presented as:

$$\begin{pmatrix}\dot{p}\\ \dot{q}\\ \dot{r}\end{pmatrix}=-I^{-1}\left\{\begin{pmatrix}p\\ q\\ r\end{pmatrix}\times\left\{I\begin{pmatrix}u\\ v\\ \omega\end{pmatrix}\right\}\right\}+I^{-1}\begin{pmatrix}L\\ M\\ N\end{pmatrix} \tag{11}$$

Where I is the inertial matrix, which is shown as:

$$I=\begin{pmatrix}I_{xx}&I_{xy}&I_{xz}\\ I_{yx}&I_{yy}&I_{yz}\\ I_{zx}&I_{zy}&I_{zz}\end{pmatrix} \tag{12}$$

$$\Delta=I_{xx}I_{zz}-I_{zz}^2 \tag{12-a}$$

$$I^{-1}=\Delta^{-1}\begin{pmatrix}I_{zz}&0&I_{xz}\\ 0&\Delta^{-1}I^{-1}{}_{yy}&0\\ I_{xz}&0&I_{xx}\end{pmatrix} \tag{12-b}$$

Where, $I_{xy}=I_{yx}=I_{zy}=I_{yz}$ is zero, because inertial matrices have no coupling effect on I_{xy}, I_{yz} and in the total flight means, and the movement is symmetric in the x-z direction [18], it means that:

$$I=\begin{pmatrix} I_{xx} & 0 & -I_{xz} \\ 0 & I_{yy} & 0 \\ -I_{xz} & 0 & I_{zz} \end{pmatrix} \quad (12\text{-c})$$

Or, in general, we can express it in the form of:

$$\dot{\omega}^{B}_{B/N}=I^{-1}\left(M_B-\omega^{B}_{B/N}\times\left(I\omega^{B}_{B/N}\right)\right) \quad (13)$$

Table 1 Variable values in simulation

Parameter	Value	Unit	Parameter	Value	Unit
I_{xx}	0.251	kg·m^2	Ω_{mr}	193.73	rad/s
I_{yy}	0.548	kg·m^2	Ω_{tr}	900.85	rad/s
I_{zz}	0.787	kg·m^2	R_{mr}	0.705	m
T_{mr}	96.766	N	R_{tr}	0.128	m
T_{tr}	4.188	N	m	9.750	kg
H_{mr}	0.337	m	k_{tr}	0.12064	m/rad
V_{imr}	4.190	m/s	k_{mr}	0.71052	m/rad
V_{itr}	5.62	m/s	Kβ	114.05	N. m
ρ	1.29	kg·m^3	A_{mr}	1.5614	m^2
H_{mr}	0.337	m	A_{tr}	0.0514	m^2
H_{tr}	0.172	m	H_{vf}	0.184	m
H_{tr}	0.172	m	C_{lavf}	2.85	(rad)$^{-1}$
S_{fx}	0.103	m^2	A_{lon}	0.210	rad
S_{fy}	0.900	m^2	B_{lat}	0.200	rad
S_{fz}	0.084	m^2	D_{lat}	0.570	rad
S_{hf}	0.011	m^2	C_{lon}	0.560	rad
S_{vf}	0.007	m^2	K_{sb}	1	n. a
τ_{sb}	0.2528	sec	τ_{mr}	0.0462	sec
k_{ped}	1	n. a	θ_{ped0}	0.143	rad
k_{col}	0.165	n. a	θ_{col0}	0.0750	rad
A_{bs}	9.720	1/s	B_{as}	10.704	1/s
C_{lahf}	2.85	(rad)$^{-1}$	g	9.781	$\frac{N}{kg}$

It should be noted that, in introducing the kinematics equations, the derivatives of the Euler angles are not orthogonal to each other [18].

$$\begin{aligned} \dot{\varnothing} &= p+qtan\theta sin\varnothing+rtan\theta cos\varnothing \\ \dot{\theta} &= qcos\varnothing-rsin\varnothing \\ \dot{\psi} &= qsin\varnothing sec\theta+rcos\varnothing\sec\theta \end{aligned} \quad (14)$$

Or, in summary, we will have:

$$\dot{\vartheta}=\begin{pmatrix}\dot{\varnothing}\\ \dot{\theta}\\ \dot{\psi}\end{pmatrix}=S^{-1}\omega^{B}_{B/N} \quad (15)$$

Where:

$$S^{-1}=\begin{pmatrix}1 & sin\varnothing tg\theta & cos\varnothing tg\theta\\ 1 & cos\varnothing & -sin\varnothing\\ 0 & sin\varnothing sec\theta & cos\varnothing sec\theta\end{pmatrix} \quad (16)$$

Using the kinematic and dynamical model of a small-scale unmanned rotorcraft, it can be described by Newton-Euler's Law as:

$$\dot{P}_N=V_N=R(\Theta)V_B \quad (17)$$

Where, $P_N=[x\ y\ z]^T$ and $R(\Theta)$ is the matrix of the rotation that is resulted from the following rotation matrix.

$$R(\Theta)=R_{\psi}(\psi)R_{\theta}(\theta)R_{\phi}(\phi)$$

$$R(\Theta)=\begin{pmatrix}C\theta C\psi & S\phi S\theta C\psi-C\phi S\psi & C\phi S\theta C\psi+S\phi S\psi\\ C\theta S\psi & S\phi S\theta S\psi+C\phi C\psi & C\phi S\theta S\psi-S\phi C\psi\\ S\theta & S\phi S\theta & C\phi C\theta\end{pmatrix} \quad (18)$$

However, in some cases, wind velocity can be neglected, but in calculating aerodynamic forces, it can be considered which is introduced according to the speed of the rotorcraft relative to the movement in the air to the fuselage speed $V_a=(u_a\ \ v_a\ \ w_a)^T$. We introduce the velocity of wind motion as an external perturbation, it is introduced with the symbol *W*, and the vector $V_{win}=(u_w\ \ v_w\ \ w_w)^T$, and consequently, the "Eq. (19)" is presented [19].

$$u_a=u-u_w,\ v_a=v-v_w,\ w_a=w-w_w \quad (19)$$

The details of the "Eq. (7)" which includes the equations of the main rotor components is introduced as:

$$\begin{aligned} X_{mr} &= -T_{mr}\sin a_s \\ Y_{mr} &= T_{mr}\sin b_s \\ Z_{mr} &= -T_{mr}\cos a_s\cos b_s \end{aligned} \quad (20)$$

Where, T_{mr} is the trust of the main rotor. The moment generated for the main rotor, used in "Eq. (10)", is expressed as [19]:

$$L_{mr} = sin(b_s)(K\beta + T_{mr} H_{mr})$$
$$M_{mr} = sin(a_s)(K\beta + T_{mr} H_{mr}) \quad (21)$$
$$N_{mr} = -P_{mr} \cdot \Omega^{-1}$$

Where, P_{mr} is the amount of total consumed power, which includes following four forces:

$$P_{mr} = P_{pr} + P_i + P_{pa} + P_c \quad (22)$$

It contains the main rotor power, the main rotor induction power, the perturbation power, the incremental power, respectively, their calculations can be followed in [19]. The value of $K\beta$ is also considered to be the effective constant of the main rotor and H_{mr} is the main distance of hub rotor.

$$P_{pr} = 0.125\rho\Omega_{mr} R_{mr}^2 C_{D0} b_{mr} c_{mr} \left((\Omega_{mr} R_{mr})^2 + 4.6(u_a^2 + v_a^2)\right)$$
$$P_i = T_{mr} v_{imr}$$
$$P_{pa} = |X_{fus} u_a| + |Y_{fus} v_a| + |Z_{fus} (w_a - v_{imr})|$$
$$P_c = -mgw_a : w_a < 0 \quad (22\text{-a})$$

2.1. Main Rotor and Moment Force

The exact value of T_{mr} can be determined as:

$$T_{mr} = 0.25\left(\rho\Omega_{mr} R_{mr}^2 k_{mr}\right)(\omega_{bldmr} - v_{imr})$$
$$v_{imr}^2 = \sqrt{\left(\hat{v}^2/2\right)^2 + \left(T_{mr}/2.\rho.A_{mr}\right)^2} - \left(\hat{v}^2/2\right) \quad (23)$$
$$\omega_{bldmr} = \omega_{rmr} + 0.67\Omega_{mr} R_{mr} \theta_{col}$$

Where, Ω_{mr} is the main rotor rotation velocity, A_{mr} is the main rotor disk area, ω_{bldmr} is the pure vertical velocity relative to the main rotor blade, v_{imr} is the induction velocity generated by the main rotor and $\hat{v}^2$ is an average variable in the calculations of the main rotor thrust, in which the method of determining the relationship is introduced in [19]. The variable ω_{rmr} is the net vertical velocity through the main rotor disk, R_{mr} is the radius of the main rotor blade and k_{mr} is the main rotor constant, which is derived from the result of multiplying the lift curve slope by the main rotor blade and the length of the tendon of the main rotor blade and the number of main rotor blades; and θ_{col} is the collective pitch angle of the main rotor blade.

2.2. Tail and Moment Rotor Force

A tail rotor is usually used to control and direct the rotorcraft and to prevent the Moment from the main rotor. Its calculation is completely identical to the original rotor and, since the tail rotor blade size is very small, its flapping effect is negligible. k_{tr} is introduced as the constant of the tail rotor which results from the multiplication of the slope of the lift curve by the blade of the tail rotor and the length of the tendon of the tail rotor blade and the number of tail rotor blades [19].

$$T_{tr} = 0.25\left(\rho\Omega_{tr} R_{tr}^2 k_{tr}\right)(\omega_{bldtr} - v_{itr})$$
$$v_{itr}^2 = \sqrt{\left(\hat{v}^2/2\right)^2 + \left(T_{tr}/2.\rho.A_{tr}\right)^2} - \left(\hat{v}^2/2\right) \quad (24)$$
$$\omega_{bldtr} = \omega_{rtr} + 0.67\Omega_{tr} R_{tr} \theta_{ped}$$
$$\theta_{ped} = k_{ped} \bar{u}_3 + \theta_{ped\,0}$$

Where, k_{ped}, $\theta_{ped\,0}$, $\bar{u}_3$ are ratio of tail rotor blade, pedal angle to rudder servo deflection when the offset value of $\bar{u}_3$ is zero, and rudder servo actuator deflection rb, espectively [19].

2.3. Fuselage Forces

The fuselage, during the flight, moves along the three directions of the X, Y, Z of fuselage frame. In "Fig. 2", the calculation algorithm is presented in which the effect of the drag forces in the X, Y and Z directions is presented by s_{fx}, s_{fy}, s_{fz} symbols, respectively.

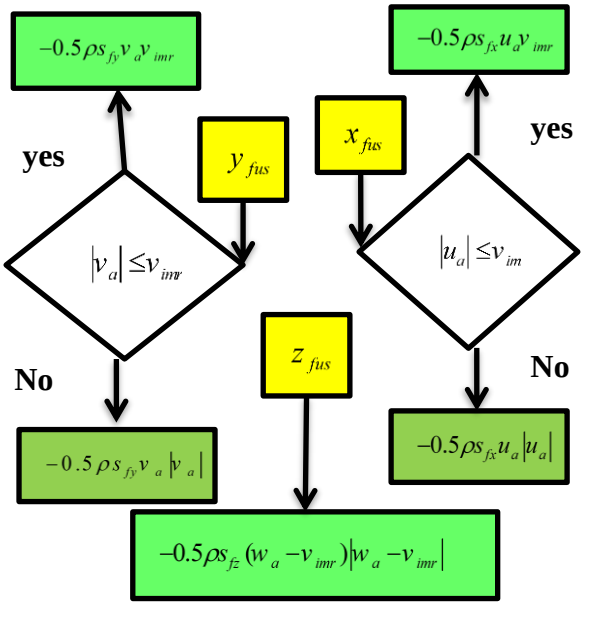

Fig. 2 Algorithm of fuselage forces.

The calculation algorithm for the Moment and vertical wing forces in the Y direction with the y_{vf} symbol is shown in "Fig. 3". We introduce α_i as the angle of attack, and the local lateral vertical velocity in the air with the symbol v_{vf} and the slope of the lift curve by c_{lavf} [19].

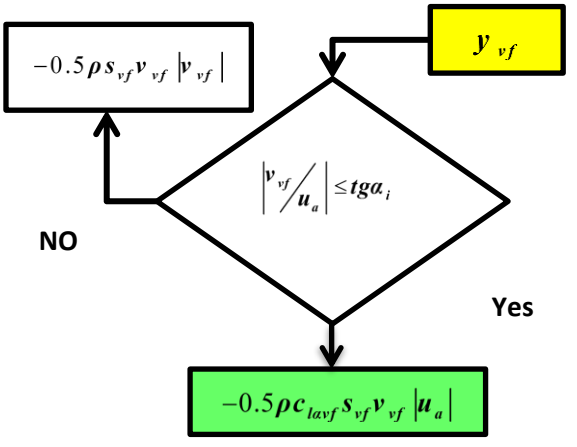

Fig. 3 Algorithm of forces and Vertical Moment of the tail.

To determine the moment and forces of the wing horizontal force shown as z_{hf} and how it is calculated, see "Fig. 4". The slope of the horizontal lift curve is introduced as c_{lahf} and the area of the horizontal area is represented by the s_{hf} [19-20].

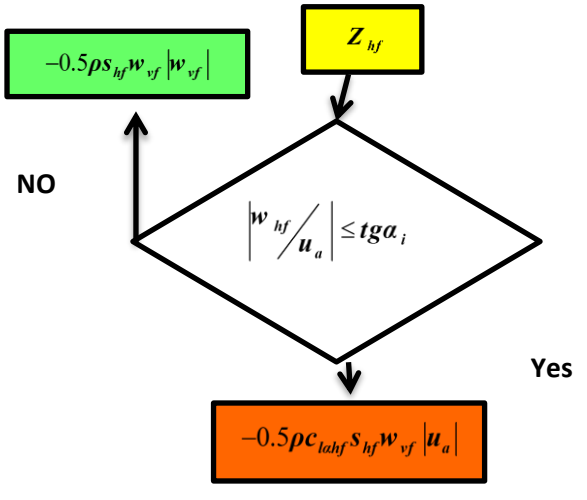

Fig. 4 Algorithm of forces and horizontal moment of the tail.

2.4. The Main Rotor Flapping Dynamics

An overview of the equations can be found in references[21-23]. The general form is:

$$\dot{a}_s = \frac{A_{lon} + k_{sb} C_{lon}}{\tau_{mr} + \tau_{sb}} u_2 + \frac{\tau_{mr} A_{bs}}{\tau_{mr} + \tau_{sb}} b_s - \frac{1}{\tau_{mr} + \tau_{sb}} \left[a_s + (\tau_{mr} + k_{sb}\tau_{sb}) q \right]$$
$$\dot{b}_s = \frac{B_{lat} + k_{sb} D_{lat}}{\tau_{mr} + \tau_{sb}} u_4 + \frac{\tau_{mr} B_{as}}{\tau_{mr} + \tau_{sb}} a_s - \frac{1}{\tau_{mr} + \tau_{sb}} \left[b_s + (\tau_{mr} + k_{sb}\tau_{sb}) p \right] \quad (25)$$

3 EXTRACTING THE POLYTOPIC MODEL

Rotorcrafts are very nonlinear systems, which have a very complex and significant dynamics. However, researchers, in order to analyze, typically produce linearized models of rotorcraft systems. In particular, a linear model approximates a special nonlinear rotorcraft system working around the operating point and signals. The general form of the nonlinear equation is presented as the following equation.

$$\dot{x} = f(x,u) \quad (26)$$

After linearization of the system we will have:

$$\Delta\dot{x} = A_i \Delta x + B_i \Delta u \quad (27)$$

Where:

$$A_i = \left.\frac{\partial f(x,u)}{\partial x}\right|_{\substack{x=x_{0i} \\ u=u_{0i}}} ; B_i = \left.\frac{\partial g(x,u)}{\partial u}\right|_{\substack{x=x_{0i} \\ u=u_{0i}}}$$
$$x^T = (u, w, q, \theta, a_s, v, p, r, \phi, b_s)$$
$$u^T = (u_1, u_2, u_3, u_4) \quad (28)$$
$$y^T = (u, w, q)$$

And $x = x_{0i}$, $u = u_{0i}$ is any desired operating point, and it is considered that the inputs are normalized to interval [1, -1]. The general case for matrices A_i and B_i are presented as:

$$A_i = \begin{bmatrix} X_u & X_w & X_q & X_\theta & X_{as} & X_v & X_p & X_r & X_\phi & X_{bs} \\ Z_u & Z_w & Z_q & Z_\theta & Z_{as} & Z_v & Z_p & Z_r & Z_\phi & Z_{bs} \\ M_u & M_w & M_q & M_\theta & M_{as} & M_v & M_p & M_r & M_\phi & M_{bs} \\ \theta_u & \theta_w & \theta_q & \theta_\theta & \theta_{as} & \theta_v & \theta_p & \theta_r & \theta_\phi & \theta_{bs} \\ A_u & A_w & A_q & A_\theta & A_{as} & A_v & A_p & A_r & A_\phi & A_{bs} \\ Y_u & Y_w & Y_q & Y_\theta & Y_{as} & Y_v & Y_p & Y_r & Y_\phi & Y_{bs} \\ L_u & L_w & L_q & L_\theta & L_{as} & L_v & L_p & L_r & L_\phi & L_{bs} \\ N_u & N_w & N_q & N_\theta & N_{as} & N_v & N_p & N_r & N_\phi & N_{bs} \\ \phi_u & \phi_w & \phi_q & \phi_\theta & \phi_{as} & \phi_v & \phi_p & \phi_r & \phi_\phi & \phi_{bs} \\ B_u & B_w & B_q & B_\theta & B_{as} & B_v & B_p & B_r & B_\phi & B_{bs} \end{bmatrix}$$

$$B_i = \begin{bmatrix} X_{u1} & X_{u2} & X_{u3} & X_{u4} \\ Z_{u1} & Z_{u2} & Z_{u3} & Z_{u4} \\ M_{u1} & M_{u2} & M_{u3} & M_{u4} \\ \theta_{u1} & \theta_{u2} & \theta_{u3} & \theta_{u4} \\ A_{u1} & A_{u2} & A_{u3} & A_{u4} \\ Y_{u1} & Y_{u2} & Y_{u3} & Y_{u4} \\ L_{u1} & L_{u2} & L_{u3} & L_{u4} \\ N_{u1} & N_{u2} & N_{u3} & N_{u4} \\ \phi_{u1} & \phi_{u2} & \phi_{u3} & \phi_{u4} \\ B_{u1} & B_{u2} & B_{u3} & B_{u4} \end{bmatrix} \quad (29)$$

More detailed explanations of the "Eq. (29)" are explained in reference [18]. The matrices produced in the equilibrium point, range from static to flight mode with the velocity up to 12 m/s in appropriate intervals and with 490 data set generated by the matrix $A_{10\times10}$ and 490 data set generated by the matrix $B_{4\times10}$. Calculation of system matrices by differentiation of "Eq. (28)" results in the following general form.

$$A_i = \begin{bmatrix} \alpha_{1,1} & \alpha_{1,2} & \alpha_{1,3} & \alpha_{1,4} & \alpha_{1,5} & \alpha_{1,6} & \alpha_{1,7} & \alpha_{1,8} & 0 & \alpha_{1,10} \\ \alpha_{2,1} & \alpha_{2,2} & \alpha_{2,3} & \alpha_{2,4} & \alpha_{2,5} & \alpha_{2,6} & \alpha_{2,7} & 0 & \alpha_{2,9} & \alpha_{2,10} \\ \alpha_{3,1} & \alpha_{3,2} & \alpha_{3,3} & 0 & \alpha_{3,5} & \alpha_{3,6} & \alpha_{3,7} & \alpha_{3,8} & 0 & \alpha_{3,10} \\ 0 & 0 & \alpha_{4,3} & 0 & 0 & 0 & 0 & \alpha_{4,8} & \alpha_{4,9} & 0 \\ 0 & 0 & \alpha_{5,3} & 0 & \alpha_{5,5} & 0 & 0 & 0 & 0 & \alpha_{5,10} \\ \alpha_{6,1} & \alpha_{6,2} & \alpha_{6,3} & \alpha_{6,4} & \alpha_{6,5} & \alpha_{6,6} & \alpha_{6,7} & \alpha_{6,8} & \alpha_{6,9} & \alpha_{6,10} \\ \alpha_{7,1} & \alpha_{7,2} & \alpha_{7,3} & 0 & \alpha_{7,5} & \alpha_{7,6} & \alpha_{7,7} & \alpha_{7,8} & 0 & \alpha_{7,10} \\ \alpha_{8,1} & \alpha_{8,2} & \alpha_{8,3} & 0 & \alpha_{8,5} & \alpha_{8,6} & \alpha_{8,7} & \alpha_{8,8} & 0 & \alpha_{8,10} \\ 0 & 0 & \alpha_{9,3} & \alpha_{9,4} & 0 & 0 & \alpha_{9,7} & \alpha_{9,8} & \alpha_{9,9} & 0 \\ 0 & 0 & 0 & 0 & \alpha_{10,5} & 0 & \alpha_{10,7} & 0 & 0 & \alpha_{10,10} \end{bmatrix}$$

$$B_i = \begin{bmatrix} b_{1,1} & 0 & 0 & 0 \\ b_{2,1} & 0 & 0 & 0 \\ b_{3,1} & 0 & 0 & 0 \\ b_{4,1} & 0 & 0 & 0 \\ 0 & b_{5,2} & 0 & 0 \\ b_{6,1} & 0 & b_{6,3} & 0 \\ b_{7,1} & 0 & b_{7,3} & 0 \\ b_{8,1} & 0 & b_{8,4} & 0 \\ 0 & 0 & 0 & 0 \\ 0 & 0 & 0 & b_{10,10} \end{bmatrix} \quad (30)$$

Figure 5 shows the dynamic model in the rotorcraft structure. In "Table 3", forces, inputs, and outputs are introduced [19].

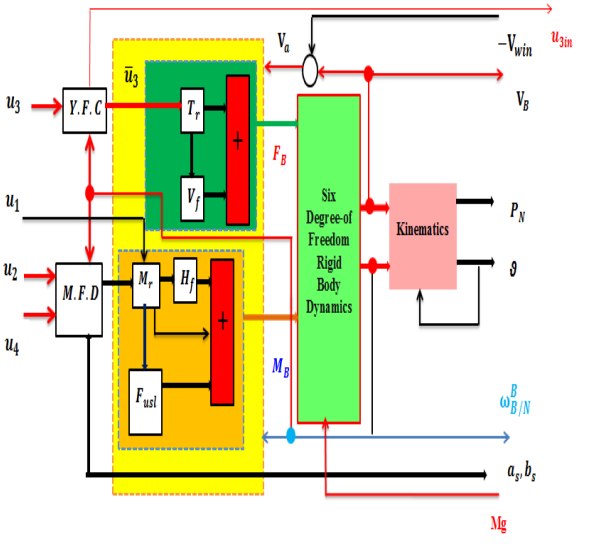

Fig. 5 Main dynamic structure of the rotorcraft.

Traceability and robust efficiency, in control of MIMO airborne vehicles, are the most important requirements for designing a stabilization control law that guarantees efficiency during real-time operations. Over the past few decades, LPV control techniques have been successful in controlling nonlinear equipment. The main importance of this technique is that using the gain-scheduled theory, the linear controller can be formulated for nonlinear systems. The main problem with LPV systems is that due to the complexity of controlling the large dimensions of variable factors, the controller's formulation is very difficult by the analysis method. However, after the development of the Linear Matrix Inequalities (LMIs), LPV problem solving with semi-described programming has become much easier [14]. In general, due to the high performance of linear systems in the control topics and the interest of the investigators in the field of control, they can bring in systems with complex nonlinear properties in linear form. The standard form of the LMI matrix is presented as:

$$F(x) = F_0 + \sum_{i=1}^{n} x_i F_i < 0 \quad (31)$$

Where, $x = [x_1, \cdots, xn]^T$ are the polynomial vector coefficients and they are also introduced as a decision vector which is unclear. The LPV system was introduced by Shamma in 1998. LPV systems are linear dynamical systems that in describing the mathematical model, they are depended on the parameters that vary over time. These parameters are generally limited and are considered to be within the set of $\Delta\mu$ and are often

assumed as a compact and convex polygon (for example, a box) [24]. In general, an LPV system can be represented as:

$$\begin{aligned} \dot{x} &= A(\mu(t))x(t) + B(\mu(t))u(t) \\ y &= C(\mu(t))x(t) + D(\mu(t))u(t) \end{aligned} \tag{32}$$

As it can be seen, "Eq. (32)" is a dynamic model of linear mode space, but their particular difference is in model matrices, which are non-deterministic and they are dependent on free parameters in the system with the condition that $u(t) \in R^{k}$ is as the input and $y(t) \in R^{l}$ as the output and $x(t) \in R^{m}$ as the state vector [25].

The linearized mode (27) with the choice of vector $\mu(t) = [\hat{x}(t)^T, \hat{u}(t)^T]^T$ as the selected path and definition $x = \hat{x} + \Delta x$ and $u = \hat{u} + \Delta u$, can be described by:

$$\Delta\dot{x} = A(\mu(t))\Delta x(t) + B(\mu(t))\Delta u(t) \tag{33}$$

$$s(\mu) = \begin{pmatrix} A(\mu(t)) & B(\mu(t)) \\ C(\mu(t)) & D(\mu(t)) \end{pmatrix} \in R^{(m+k)\times(m+l)} \tag{34}$$

4 CONTROL DESIGN

Lem1: Switching systems are introduced in the following series [26]:

$$S_{ss} = \left\{ \mu : R \geq 0 \to \{0,1\}^{N} : \sum_{i=1}^{N} \mu_i = 1 \right\} \tag{36}$$

According to **lem1**:

$$\begin{aligned} S(\mu) &= CONVEX\{S(\mu_1), S(\mu_2), \ldots, S(\mu_N)\} \\ S(\mu) &= \sum_{i=1}^{N} \boldsymbol{\beta}_i S(\mu_i) \end{aligned} \tag{37}$$

Where, N is the number of polytypic vertices, and it is considered that $\sum_{i=1}^{N} \boldsymbol{\beta}_i = 1$ and $\boldsymbol{\beta}_i \geq 0$ by saying that $S_i = (A_i, B_i)$, is calculated in our ultimate goal and determination of the matrix K as a constant state feedback control gain matrix. It means:

$$\Delta u = -K\Delta x \tag{38}$$

In the following, using the control law (38) and applying it to "Eq.(33)", which is actually equal to applying the control rule $u = \hat{u} + \Delta u$ to the nonlinear plant, an appropriate estimate of the matrix (A_i, B_i) can be introduced [27] as:

$$A_i = \hat{A}_i + \delta A_i ; B_i = \hat{B}_i + \delta B_i \tag{39}$$

Where, $i \in \{1,2,3,\ldots,N\}$ and $\hat{B}_i, \hat{A}_i$ are the estimated matrices for the nominal model of the vertices of the ploytopic model. Now we have:

$$\Delta\dot{x} = [A(\mu(t)) - B(\mu(t))K]\Delta x(t) \approx \sum_{i=1}^{N} \boldsymbol{\beta}_i (A_i - B_i K)\Delta x(t) \tag{40}$$

It can be reformulated:

$$\Delta\dot{x} = \sum_{i=1}^{N} \boldsymbol{\beta}_i (A_i - B_i K)\Delta x(t) = \sum_{i=1}^{N} \boldsymbol{\beta}_i A_{cli}\Delta x(t) \tag{41}$$

Using "Eq. (39) in (41)", we obtaine [28]:

$$\Delta\dot{x} = \sum_{i=1}^{N} \boldsymbol{\beta}_i \hat{A}_{cli}\Delta x + \delta\Delta x \tag{42}$$

Where, $\hat{A}_{cli}$ is the estimated closed-loop system matrix for the nominal closed-loop system matrix A_{cli} . The following lemma gives the asymptotically stability condition.

Lem2 [28]**:**

If there are the following positive definite matrices:

$$X^T = X,\ Y^T = Y;\ X, Y \geq 0 \tag{43}$$

Such that the following LMIs are satisfied for vertices models, then polytopic LPV model is asymptotically stable under the state feedback control with the control matrix gaine $K = MX^{-1}$.

$$M^T \hat{B}_i^T + \hat{B}_i M - \hat{A}_i^T X - X\hat{A}_i^T > \lambda Y \tag{44}$$

5 SIMULATION

Velocity control is examined in this section.. The speed ranges from near to zero meters (near hover) per second to twelve meters per second are generated at appropriate distances. The block diagram depicted in "Fig. 6" shows how to apply the equations and how to use the proposed controller in a flight system. In the following, the simulation results for speed control are presented in several scenarios. In general, the most important and the main state for controlling the movement of rotorcraft is velocity in the longitudinal direction. With a full application of fuselage force equations, the main rotors and tail, the flapping equations, the vertical fin and tail, and their great impact on each other causes initial differences in the outputs and stability of the velocity. This part is one of our most important research features because in all cases investigated based on research knowledge, in all cases, some parts of the interrupted

forces are eliminated or the form of separation of internal and external layers of research is focused which makes it partially simple. That is, by focusing on the inner or outer layer, some of the forces influencing each other are practically eliminated and the percentage of those resulting influential forces is effectively eliminated. The greatest impact of interference on lateral speed control is understandable due to its existential type. However, the goal we set for ourselves was the ability to control the synchronous velocity of the speeds along with the longitudinal, altitudinal, lateral directions, which the problems in this domain were a major challenge in controlling the velocity of the rotorcraft flight system. [19], [23], describe the flight areas in different classes. According to "Eq. (45) and Table 2", we introduce the velocity regions generated from the Near-Hover (almost stationary) to the calculated maximum velocity, which is 12 m/s. According to "Table 2", we present the simulation scenarios as shown in "Fig. 7".

Table 2 The introduction of speed areas

State	areas	Speed araes
A	Near Hover: (N.H)	$0 < u \leq 3$
B	Low Speed: (L.S)	$3 < u \leq 7$
C	High Speed: (H.S)	$7 < u$

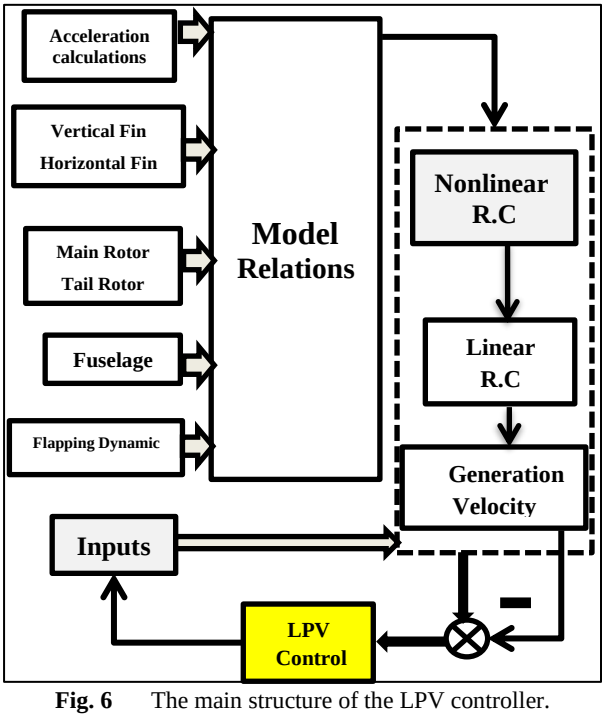

Fig. 6 The main structure of the LPV controller.

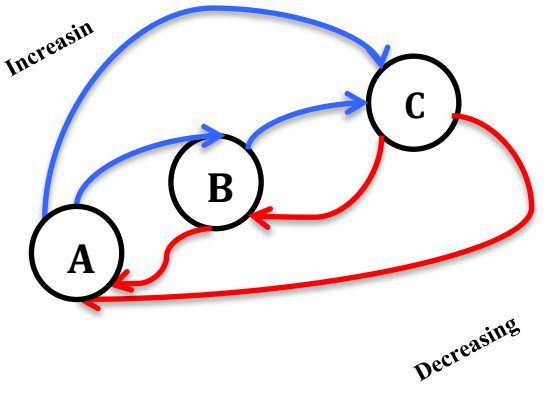

Fig. 7 Introducing simulation scenario.

In the first scenario, the aim is to control the incremental velocities and in the second scenario, the goal of the reducing velocity is examined.

5.1. First Scenario: Incremental Modes

- The first goal: in this section, the increasing speed from -A to B is examined
- The second goal: the incremental velocity from the minimum velocity of A to the maximum velocity of B would be examined.
- The third goal: the incremental velocity from the minimum velocity of B to the minimum velocity of C would be examined.
- The fourth goal: In this case, the sudden increase is examined and analyzed, which is the change of state from A to C, which is one of the most difficult modes of the velocity control.

However, in reference [19], the incremental velocity was analyzed by analyzing experimental results and comparing them with simulation results, but it did not study the method of the speed stability control, and also the simulation results were introduced with a relatively high error rate and there is no mention of speed control in decrement mode. In the first goal, we examine the minimum velocity of the near-hover state, namely mode A, to the minimum velocity of the mode B with the introduction of Stability Speed Control (S.S.C) and Speed Stability Error (S.S.E) the description of the figures.

5.1.1. In the first scenario of the first goal

Figure 8 controls the longitudinal, lateral, and altitudinal velocities and "Fig. 9" presents the speed stability error.

$$\boldsymbol{Min\ speed\ u,v,w(N.H) = 0.1, 0, 0\ m/s}$$
$$\boldsymbol{Min\ speed\ u,v,w(L.S) = 3.1, 0, 0\ m/s}$$

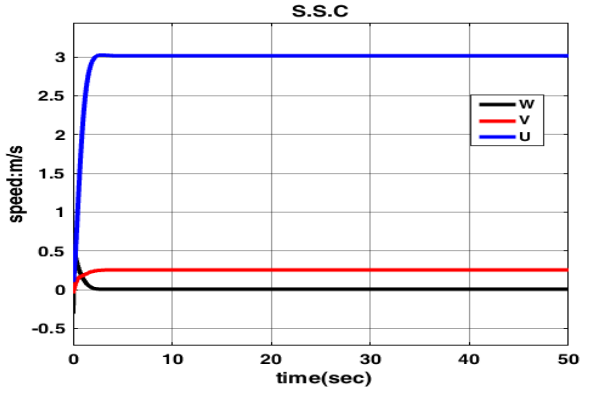

Fig. 8 The response of speed: the first goal of the first scenario, **(U):** solid blue line longitudinal, **(V):** solid red line lateral, **(W)**: solid black line altitudinal.

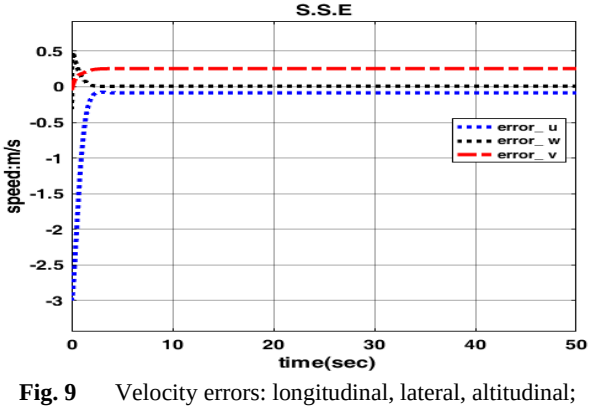

Fig. 9 Velocity errors: longitudinal, lateral, altitudinal; **(U):** dashed blue line Longitudinal, **(V):** dashed red line lateral, **(W):** dashed black line altitudinal, first goal of the first scenario.

5.1.2. In the first scenario of the second goal

The minimum velocity of the mode A to the maximum speed of the mode B is considered in this part. In "Fig. 10", the output of the stable state is shown, and in "Fig. 11", the target error condition is presented.

$$\boldsymbol{Min\ speed\ u,v,w(N.H) = 0.1\ ,0\ ,0\ m/s}$$
$$\boldsymbol{Max\ speed\ u,v,w(L.S) = 7,0\ ,0\ m}/\mathrm{s}$$

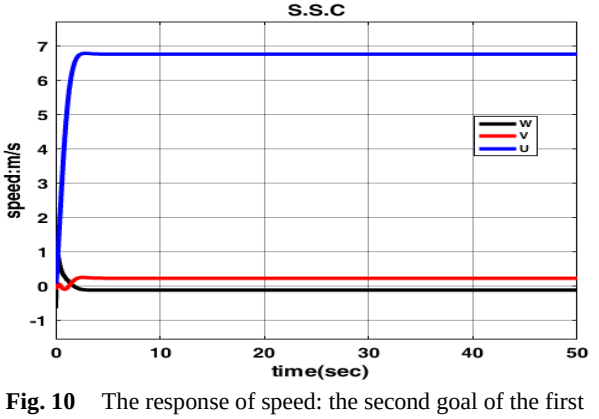

Fig. 10 The response of speed: the second goal of the first scenario; **(U):** solid blue line longitudinal, **(V)**: solid red line lateral, **(W)**: solid black line altitudinal.

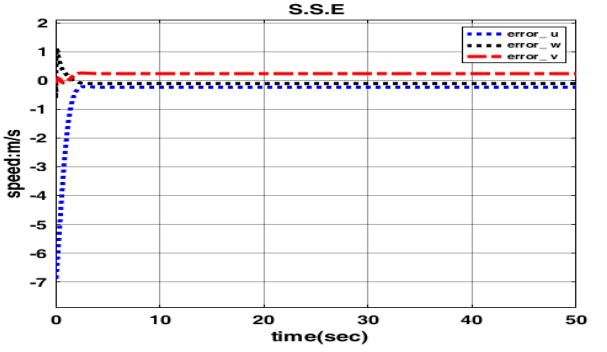

Fig. 11 Velocity errors: longitudinal, lateral, altitudinal; **(U):** dashed blue line Longitudinal, **(V):** dashed red line lateral, **(W):** dashed black line altitudinal, the second goal of the first scenario.

5.1.3. In the first scenario of the third goal

In "Fig. 12", the output of the stable state, and in "Fig. 13" the error condition of the third goal of the first scenario are presented.

$$\boldsymbol{Min\ speed\ u,v,w(L.S) = 3.1\ ,0\ ,0\ m/s}$$
$$\boldsymbol{Min\ speed\ u,v,w(H.S) = 7.1,0\ ,0\ m/s}$$

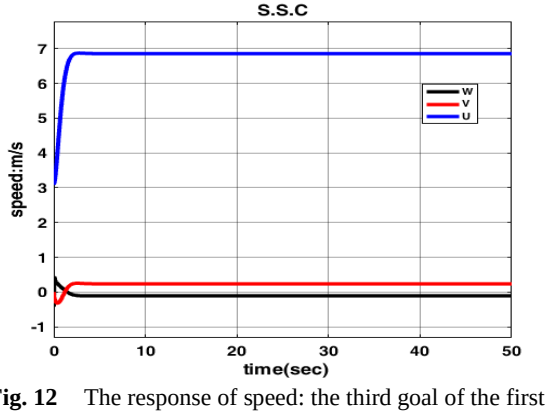

Fig. 12 The response of speed: the third goal of the first scenario; **(U)**: solid blue line longitudinal, **(V):** solid red line lateral, **(W):** solid black line altitudinal,

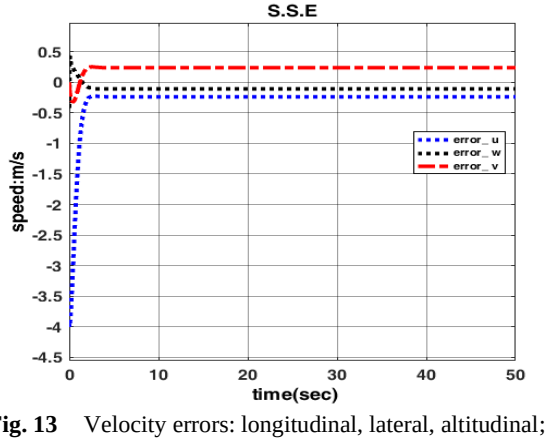

Fig. 13 Velocity errors: longitudinal, lateral, altitudinal; **(U):** dashed blue line Longitudinal, **(V):** dashed red line latera, **(W):** dashed black line altitudinal, the third goal of the first scenario.

5.1.4. In the first scenario of the fourth goal

In this goal, we examine the minimum velocity of the mode A to the maximum velocity of the mode C. In "Figs. 14 and 15", we have presented speed control and speed stability error, respectively.

$$\boldsymbol{Min\ speed\ u,v,w(N.H) = 0.1\ ,0\ ,0\ m/s}$$
$$\boldsymbol{Max\ speed\ u,v,w(H.S) = 12,0\ ,0\ m/s}$$

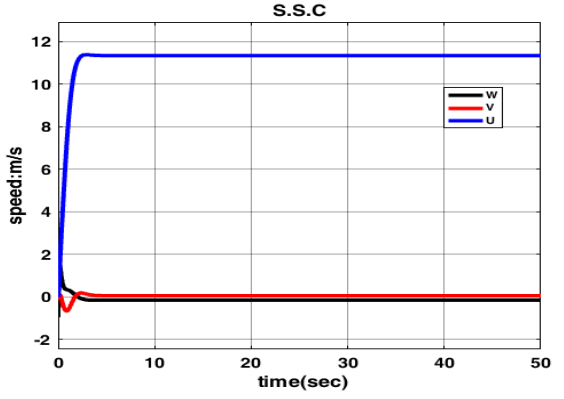

Fig. 14 The response of speed: the fourth goal of the first scenario; **(U)**: solid blue line longitudinal, **(V)**: solid red line lateral, **(W)**: solid black line altitudinal.

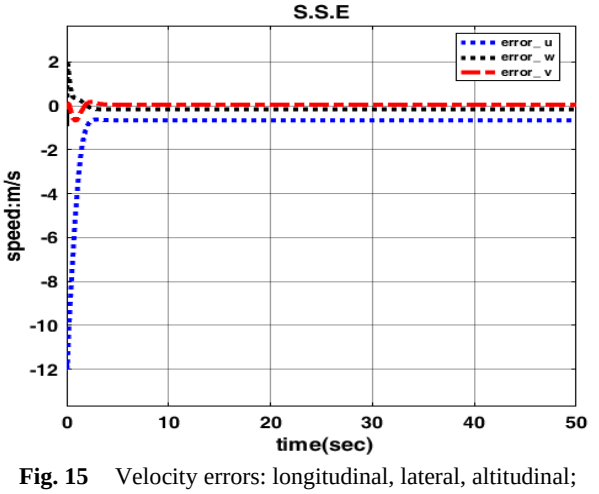

Fig. 15 Velocity errors: longitudinal, lateral, altitudinal; **(U):** dashed blue line Longitudinal, **(V):** dashed red line lateral, **(W):** dashed black line altitudinal, the fourth goal of the first scenario.

5.2. The Second Scenario: Decreasing Modes

5.2.1. The First goal: C to B

In this case, the velocity check is from the state of the maximum of the mode C to the maximum velocity of the mode B, and you can see the velocity control outputs in "Fig. 16" and the velocity control error in "Fig. 17".

$$\boldsymbol{Max\ speed\ u,v,w(H.S) = 12\ ,0\ ,0\ m/s}$$
$$\boldsymbol{Max\ speed\ u,v,w(L.S) = 7,0\ ,0\ m/s}$$

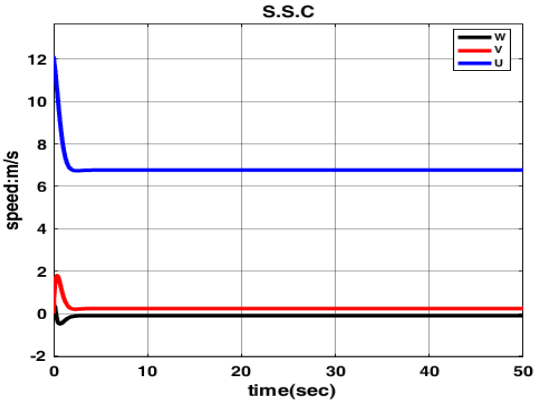

Fig. 16 The response of speed: the first goal of the second scenario; **(U):** solid blue line longitudinal, **(V):** solid red line lateral, **(W):** solid black line altitudinal.

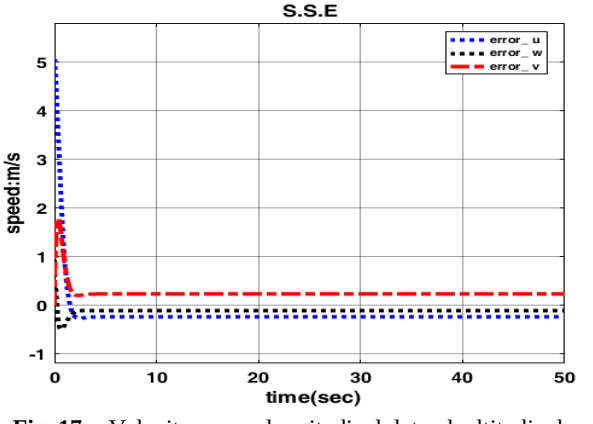

Fig. 17 Velocity errors: longitudinal, lateral, altitudinal; **(U):** dashed blue line Longitudinal, **(V):** dashed red line lateral, **(W):** dashed black line altitudinal, the first goal of the second scenario.

5.2.2. The second goal: C to B

We examine, in this goal, the highest velocity of the mode C to the lowest velocity of the mode B. Figures 18 and 19 show the velocity control of the stability of this target and the state error of the situation, respectively.

$$\boldsymbol{Max\ speed\ u,v,w(H.S) = 12,0\ ,0\ m/s}$$
$$\boldsymbol{Min\ speed\ u,v,w(L.S) = 3.1,0\ ,0\ m/s}$$

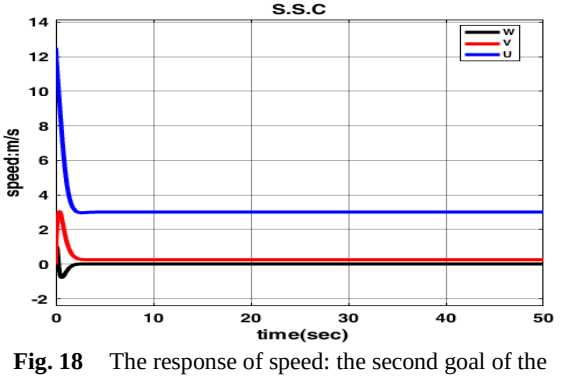

Fig. 18 The response of speed: the second goal of the second scenario; **(U):** solid blue line longitudinal, **(V):** solid red line lateral, **(W):** solid black line altitudinal

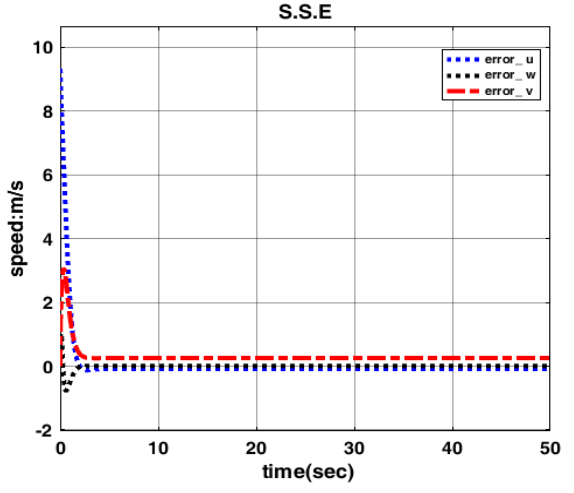

Fig. 19 Velocity errors: longitudinal, lateral, altitudinal; **(U):** dashed blue line Longitudinal, **(V):** dashed red line lateral, **(W):** dashed black line altitudinal, the second goal of the second scenario.

5.2.3. The third goal: C to A

In this goal, we examine the highest velocity of the mode C to the lowest velocity of the mode A, which is the worst-case stability state control in a decreasing state. This situation is triggered by unwanted conditions through an operator to a rotorcraft. Figures 19 and 20, show the stability velocity control of this target and the state error of this situation, respectively.

$$\boldsymbol{Max\ speed\ u,v,w(H.S) = 12\ ,0\ ,0\ m/s}$$
$$\boldsymbol{Min\ speed\ u,v,w(N.H) = 0.1,0\ ,0\ m/s}$$

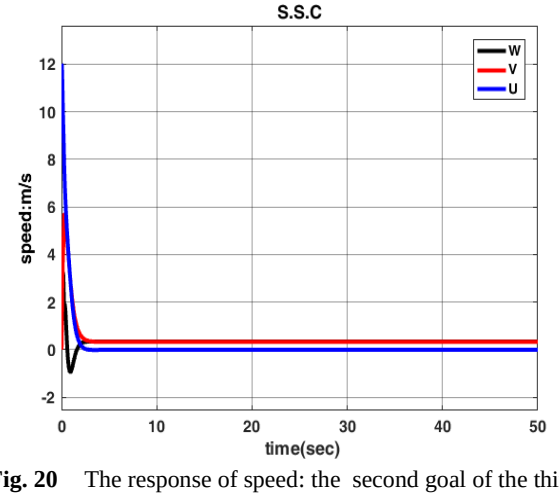

Fig. 20 The response of speed: the second goal of the third scenario; **(U)**: solid blue line longitudinal, **(V)**: solid red line lateral, **(W)**: solid black line altitudinal.

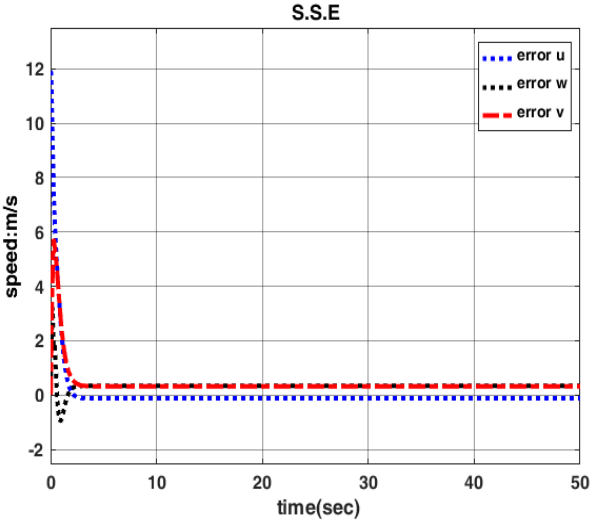

Fig. 21 Velocity errors: longitudinal, lateral, altitudinal; **(U):** dashed blue line Longitudinal, **(V):** dashed red line lateral, **(W):** dashed black line altitudinal, the third goal of the second scenario.

In "Table 3", the scenario of the incremental state and the scenario of the decreasing state and their goals are specified, and the matching errors are also presented. In this research and the proposed method, $\lambda = 0.7$ is obtained for the designed controller. The matrix k is the controller of the matrix $[k]_{4*10}$ and the matrix $[p]_{10*10}$. In "Figs 22-25", we present the control inputs. First scenario: incremental modes. In all shapes the first input is the black line and the second input is the blue line and the third input is the red line and the fourth input is the green line

Table 3 the scenario of the incremental State and scenario of decreasing state and their goals

scenario 1 Increasing States	Error u	Error v	Error w
Objective 1	-0.08652	0.2544	0.007387
Objective 2	-0.2336	0.2369	-0.1064
Objective 3	-0.2397	0.2356	-0.1086
Objective 4	-0.6625	0.0458	-0.1629
Senario2 Deceasing States			
Objective 1	-0.2336	0.2369	-0.1064
Objective 2	-0.08652	0.2544	0.007387
Objective 3	-0. 1124	0.3236	0.341

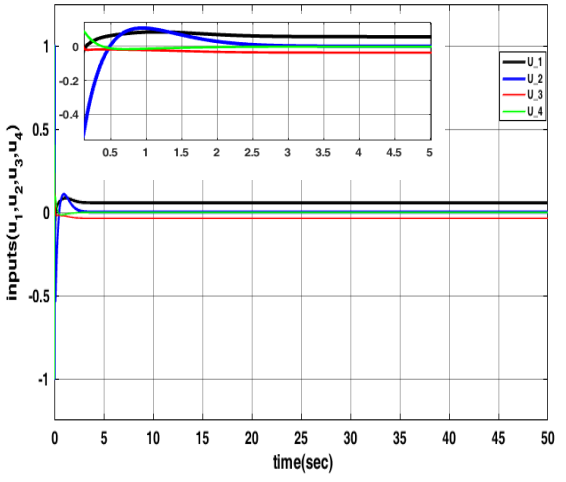

Fig. 22 Control effort: for scenario1 & Objective1; input 1: solid black line, input 2: solid blue line, input 3: solid red line, input 4: solid green line.

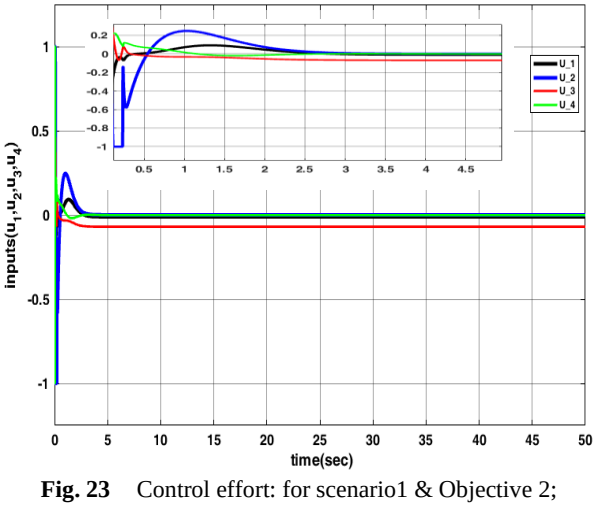

Fig. 23 Control effort: for scenario1 & Objective 2; input 1:solid black line, input 2:solid blue line, input 3: solid red line, input 4:solid green line.

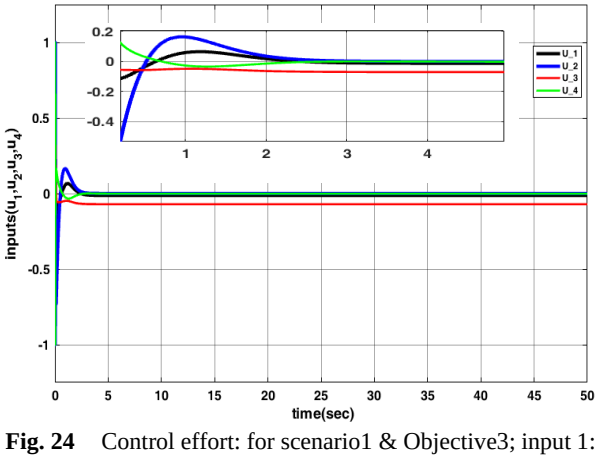

Fig. 24 Control effort: for scenario1 & Objective3; input 1: solid black line, input 2: solid blue line, input 3: solid red line, input 4: solid green line.

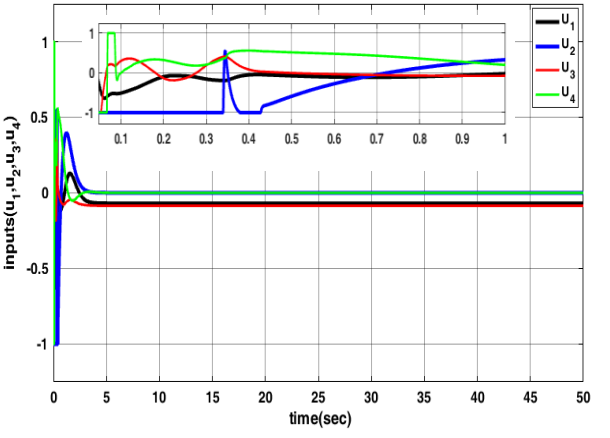

Fig. 25 Control effort: for scenario1 & Objective4; input 1: solid black line, input 2: solid blue line, input 3: solid red line, input 4:solid green line.

In "Figs 26-28", we present the control inputs. The Second Scenario: Decreasing modes. In all shapes the first input is the black line and the second input is the blue line and the third input is the red line and the fourth input is the green line.

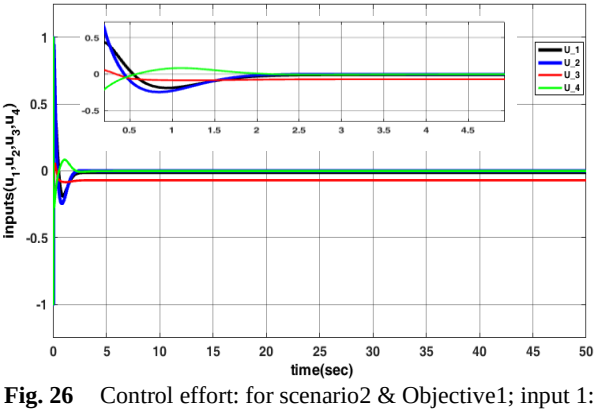

Fig. 26 Control effort: for scenario2 & Objective1; input 1: solid black line, input 2:solid blue line, input 3: solid red line, input 4: solid green line.

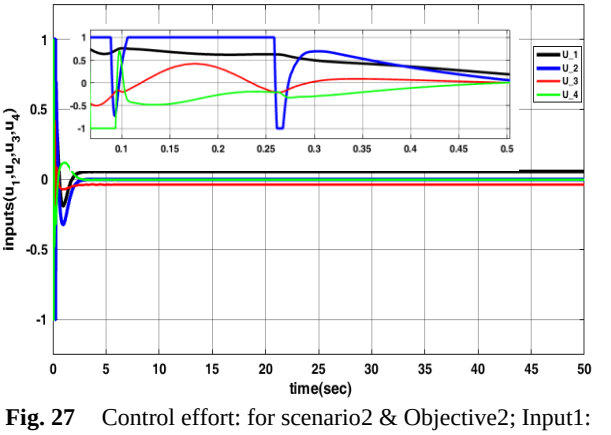

Fig. 27 Control effort: for scenario2 & Objective2; Input1: solid black line, input 2: solid blue line, input 3: solid red line, input 4: solid green line.

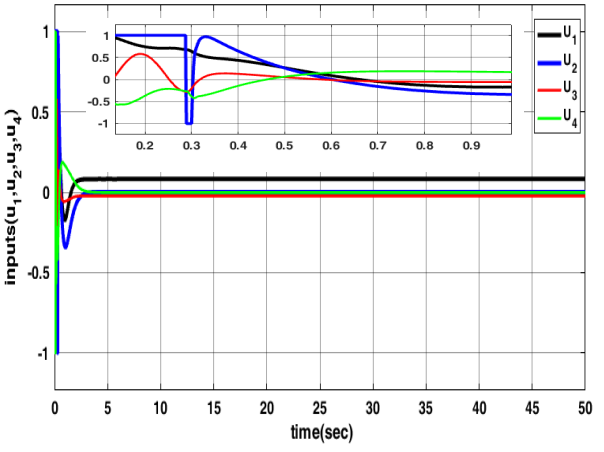

Fig. 28 Control effort: for scenario2 & Objective3; input 1: solid black line, input 2: solid blue line, input 3: solid red line, input 4: solid green line.

5 CONCLUSION

In this study, a Polytopic LPV control design, for the velocity controller stability of an unmanned rotorcraft is conducted. The optimum performance for the stability of the designed controller demonstrates the superior capability of this controller over the conventional controller. However, in this investigation, the effect of flapping forces and the impact of lateral forces are also considered and the effectiveness of the equations of these forces was also applied to the system. In this design, the performance of adaptation with different scenarios under different conditions is well illustrated with a very low error rate of this stability. This research can be the key to many of the eliminated forces in future researches.

6 LIST OF SYMBOLS

$$K = \begin{pmatrix} 1.201 & -0.6075 & -1.360 & -7.950 & 3.028 & 0.1223 & 1.0189 & 3.3961 & 2.398 & 2.414 \\ -9.091 & -2.196 & 18.657 & 69.383 & 200.80 & -0.7615 & 0.0758 & 1.7319 & -4.5015 & 0.0032 \\ -0.3483 & -0.2257 & 0.5142 & 2.114 & 0.0864 & 0.3422 & 0.651 & -0.727 & 2.664 & 11.275 \\ 4.649 & 0.389 & -1.522 & -27.776 & 4.887 & 6.595 & 21.432 & 12.473 & 68.477 & 226.766 \end{pmatrix}$$

$\gamma_{LPV} = 0.7$

symbol	Interpretation	unit
M_r	Main Rotor	-----
M_B	Aerodynamic moment vector	------
b_{mr}	Main rotor blade number	-----
A_{lon}	Linkage gain ratio of θ_{cycas} to u_2	rad
C_{lon}	Linkage gain ratio of stabilizer bar cyclic change to u_2	rad
k_{sb}	Ratio of main rotor blade cyclic pitch to stabilizer bar flapping	Na
τ_{mr}	Time constant of bare main rotor	s
τ_{sb}	Time constant of stabilizer bar	s
A_{bs}	Coupling effect from b_s to a_s	1/s
T_r	Tail Rotor	N
H_f	Horizontal fin	m
M_r	Main Rotor	
M_B	Aerodynamic moment vector	---
ρ	Air density	$Kg.m^3$
A_{lon}	Linkage gain ratio of θ_{cycas} to u_2	rad
C_{lon}	Linkage gain ratio of stabilizer bar cyclic change to u_2	rad
k_{sb}	Ratio of main rotor blade cyclic pitch to stabilizer bar flapping	Na
τ_{mr}	Time constant of bare main rotor	s
τ_{sb}	Time constant of stabilizer bar	s
A_{bs}	Coupling effect from b_s to a_s	1/s
B_{lat}	Linkage gain ratio of θ_{cycbs} to u_4	rad
D_{lat}	Linkage gain ratio of stabilizer bar cyclic change to u_4	rad
B_{as}	Coupling effect from a_s to b_s	1/s
C_{D0}	Drag coefficient of main rotor blade	-----
θ_{ped0}	Offset of $\theta_{ped}$when $\bar{u}_3$is zero	rad
θ_{col0}	Offset of $\theta_{col}$when u_1 is zero	rad
Xfus, Yfus, Zfus	Aerodynamic forces generated by fuselage	N
θ_{ped}	Collective pitch angle of tail rotor blade	rad
θ_{col}	Collective pitch angle of main rotor blade	rad

symbol	Interpretation	unit
u_1	Normalized collective pitch servo input(-1,1)	---
u_2	Normalized elevator servo input (−1, 1)	----
u_3	Normalized rudder servo input (−1, 1)	----
u_4	Normalized aileron servo input (−1, 1)	------
Y.F.C	Yaw rate Feedback Controller	---------

M.F.D	Min rotor Flapping Dynamic	---------
F_{usl}	Fuselage	N
$\bar{u}_3$	Actuator deflection	rad
u_{3in}	Intermediate state in yaw rate feedback	rad
v_a	Velocity vector relative to the air	m/s
m	Helicopter mass	kg
g	Local acceleration of gravity	m/s^2
F_B	Aerodynamic force vector	N
V_{win}	Wind gust velocity vector	m/s
V_B	Velocity vector body frame	m/s
P_N	Local NED position vector	m
V_f	Vertical fin	m
T_r	Tail Rotor	N
H_f	Horizontal fin	m

REFERENCES

[1] Avila Vilchis, J. C., Brogliato, B., Dzul, A., and Lozano, R., Nonlinear Modelling And Control of Helicopters, Automatica, Vol. 39, No. 9, 2003, pp. 1583–1596, DOI :10.1016/S0005-1098(03)00168-7.

[2] Gadewadikar, J., Lewis, F. L., Subbarao, K., and. Chen, B. M., Structured H∞ Command and Control-Loop Design for Unmanned Helicopters, J. Guid. Control. Dyn., Vol. 31, No. 4, 2008, pp. 1093–1102, DOI: 10.2514/1.31377.

[3] Tijani, I. B., Akmeliawati, R., Legowo, A., Budiyono, A., and Muthalif, A. G. A., H∞ Robust Controller for Autonomous Helicopter Hovering Control, Aircr. Eng. Aerosp. Technol., Vol. 83, No. 6, 2011, pp. 363–374, DOI: 10.1108/00022661111173243.

[4] Hongwei, Z., Xuehua, Z., and Bao, Z., System Dynamics Approach to Urban Water Demand Forecasting, Trans. Tianjin Univ., Vol. 15, No. 1, 2009, pp. 70–74, DOI: 10.1007/s12209-009-0014-5.

[5] Khizer, A. N., Yaping, D., Amjad Ali, S., and Xiangyang, X., Stable Hovering Flight for a Small Unmanned Helicopter Using Fuzzy Control, Math. Probl. Eng., Vol. 2014, Article ID 208253, 17 page, 2014, .DOI: 10.1155/2014/208253.

[6] Li, R., Chen, M., Wu, Q., and Liu, J., Robust Adaptive Tracking Control for Unmanned Helicopter with Constraints, Int. J. Adv. Robot. Syst., Vol. 14, No. 3, 2017, pp. 1–12,DOI: 10.1177/1729881417712621.

[7] Razzaghian, A., Robust Nonlinear Control Based on Disturbance Observer for a Small-Scale Unmanned Helicopter, J. Nonlinear Anal. Appl., Vol. 2017, No. 2, 2017, pp. 122–131, DOI: 10.5899/2017/jnaa-00390.

[8] Ma, R., Ding, L., and Wu. H., Dynamic Decoupling Control Optimization for a Small-Scale Unmanned Helicopter, J. Robot., Vol. 2018, Article ID 9897684, 12 pages, 2018, DOI: 10.1155/2018/9897684.

[9] Horn, J. F., Non-linear Dynamic Inversion Control Design for Rotorcraft, Aerospace, Vol. 6, No. 3, 2019, pages 38, DOI: 10.3390/aerospace6030038.

[10] Kun, D. W., Hwang, I., Linear Matrix Inequality-Based Nonlinear Adaptive Robust Control of Quadrotor, J. Guid. Control. Dyn., Vol. 39, No. 5, 2016, pp. 996–1008,DOI: 10.2514/1.G001439.

[11] Patterson, B. W., A Linear Parameter Varying Control Methodology for Reduction of Helicopter Higher Harmonic, Master of Science in Aeronautics and Astronautics, Massachusetts Institute of Technology, 2016.

[12] Mohammed, R. H., Comparative Study and Robustness Analysis of Quadrotor Control in Presence of Wind Disturbances, Vol. 12, No. 2, 2019, pp. 27–37.

[13] Lin, Z., Gain Scheduling of Aircraft Pitch Attitude and Control of Discrete, Affine, Linear Parametrically Varying Systems, Ph.D. Dissertation, Iowa State University, 2002.

[14] Jafar, A., Bhatti, A. I., Ahmad, S. M., and Ahmed, N. Robust Gain-Scheduled Linear Parameter-Varying Control Algorithm for a Lab Helicopter: A Linear Matrix Inequality–Based Approach, Proc. Inst. Mech. Eng. Part I J. Syst. Control Eng., Vol. 232, No. 5, 2018, pp. 558–571,DOI: 10.1177/0959651818759861.

[15] Da Ponte Caun, R., Assunção, E., Minhoto Teixeira, M. C., and Da Ponte Caun, A., LQR-LMI Control Applied to Convex-Bounded Domains, Cogent Eng., Vol. 5, No. 1, 2018, pp. 1–27,DOI: 10.1080/23311916.2018.1457206.

[16] Kasnakoğlu, C., Investigation of Multi-Input Multi-Output Robust Control Methods to Handle Parametric Uncertainties in Autopilot Design, PLoS One, Vol. 11, No, 2016, pp. 1–36,DOI: 10.1371/journal.pone.0165017.

[17] Raptis, I. A., Linear and Nonlinear Control of Unmanned Rotorcraft, Ph.D. Dissertation, University of South Florida, 2010.

[18] Ren, B., Ge, S. S., Chen, C. C., Fua, H., and Lee, T. H., Modeling, Control and Coordination of Helicopter Systems, 1rd ed, Springer New York Dordrecht Heidelberg London, ISBN: 9781461415633, 2012.

[19] Cai, G., Chen, B. M., and Lee, T. H., Unmanned Rotorcraft Systems,Springer London Dordrecht Heidelberg New York British, ISBN 978-0-85729-635-1, 2011.

[20] Zhou, B., Lu, X., Tang, S., and Zheng, Z., Nonlinear System Identification and Trajectory Tracking Control for a Flybarless Unmanned Helicopter: Theory and Experiment, Nonlinear Dyn., Vol. 96, No, 5, 2019, DOI: 10.1007/s11071-019-04923-9.

[21] Liu, C., Advanced Control for Miniature Helicopters: Modelling, Design and Fight Test, Ph.D. Dissertation, Department of Aeronautical and Automotive Engineering Loughborough University, 2011.

[22] Johnson, W., Rotorcraft Aeromechanics, 1rd ed, Cambridge University Press, ISBN: 978-1107606913, 2006.

[23] Mettler, B., Identification Modeling and Characteristics of Miniature Rotorcraft, Springer US, 2003, ISBN 978-1-4757-3785-1 .

[24] Shamma, J. S., Analysis and Design of Gain Scheduled Control Systems, Ph.D. Dissertation, Massachusetts Institute of Technology, Dept. of Mechanical Engineering, 1988.

[25] Petres, Z., Polytopic Decomposition of Linear Parameter-Varying Models by Tensor-Product Model Transformation, Ph.D. Dissertation, Budapest University of Technology, 2006.

[26] Souley, A. H., Boutat-Baddas, L., Becis-Aubry, Y., and Darouach. M., H-Infinity Control of a Scara Robot Using Polytopic LPV Approach,14th Mediterranean Conference on Controland Automation, DOI:10.1109/MED.2006.328836:, 2006.

[27] Kazemi, M. H., Abolhasani, J., Uncertain LPV Modeling of Power Systems using PCA-Based Parameter Set Mapping for Robust PSS Designing, TABRIZ J. Electr. Eng., Vol. 48, No. 2, pp. 455–466, 2018.

[28] Duan, G. R., Yu, H. H., LMIs in Control Systems: Analysis, Design and Applications, 1rd ed, CRC press, ISBN: 978-1466582996, 2012.